Microsc. Microanal. 7, 178–192, 2001
DOI: 10.1007/s100050010082

Microscopy AND Microanalysis

Castaing's Electron Microprobe and Its Impact on Materials Science

Dale E. Newbury

Surface and Microanalysis Science Division, National Institute of Standards and Technology, MS 8371, 100 Bureau Drive, Gaithersburg, MD 20899-8371

Abstract: The development of the electron microprobe by Raymond Castaing provided a great stimulus to materials science at a critical time in its history. For the first time, accurate elemental analysis could be performed with a spatial resolution of 1 μm, well within the dimensions of many microstructural features. The impact of the microprobe occurred across the entire spectrum of materials science and engineering. Contributions to the basic infrastructure of materials science included more accurate and efficient determination of phase diagrams and diffusion coefficients. The study of the microstructure of alloys was greatly enhanced by electron microprobe characterization of major, minor, and trace phases, including contamination. Finally, the electron microprobe has proven to be a critical tool for materials engineering, particularly to study failures, which often begin on a micro-scale and then propagate to the macro-scale with catastrophic results.

Key words: electron microprobe, electron probe microanalyzer, failure analysis, materials science, phase diagram, X-ray microanalysis

Introduction

Raymond Castaing, in conjunction with his thesis supervisor, Professor A. Guinier, presented the first paper on the electron microprobe, entitled "Application of electron probes to metallographic analysis," at the First International Congress of Electron Microscopy held in Delft, the Netherlands, in 1949. They described an instrument in which a static electron beam was focused to form a probe approximately 1 μm in diameter that was directed at a thick target to locally excite characteristic X-rays for spectrometric measurement. The area of interest could be selected with the aid of an optical microscope. This seminal paper marked the *practical* beginning of the field of electron beam microanalysis, and indeed it laid the foundation of the much broader field of instrumental microanalysis. As such, it is interesting to note that the focus of the paper was directed to electron probe applications in metallography, the study of the microstructure of metals and alloys, a branch of the field we know today as materials science. In 1949, the term "materials science" would not have been recognized, rather the field was known instead by the distinct and separate disciplines of metallurgy, ceramics, glass, and polymers. (Composite materials, a materials topic of great importance today, were not yet recognized.) Workers in any of these fields would have readily understood the importance of Castaing's breakthrough in establishing practical microanalysis. Beginning in the 1880s, the techniques of metallography developed by Sorby in England, Martens in Germany, Os-

Received November 1, 1999; accepted January 19, 2000.

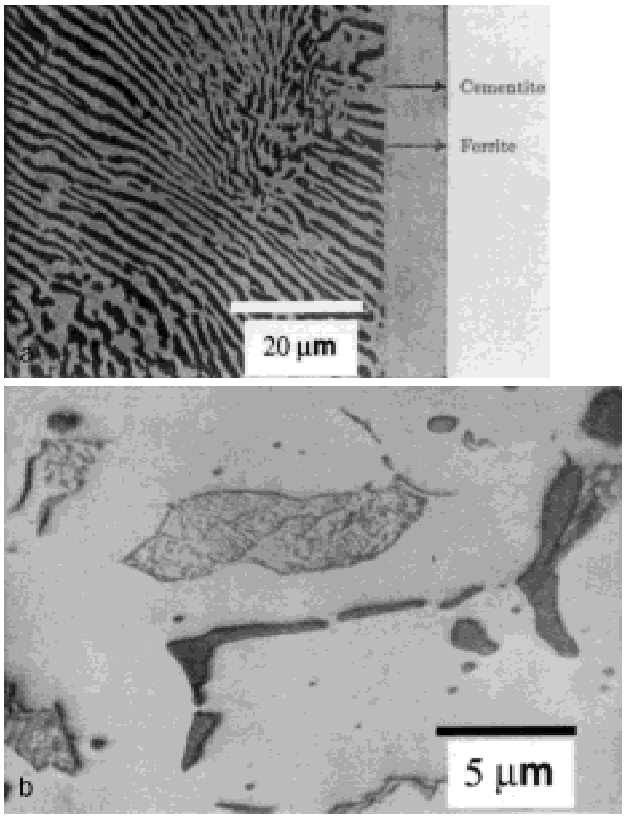

Figure 1. a: Structure of pearlite at high magnification as revealed by metallographic preparation, chemical etching, and optical microscopy (Sauveur, 1912). **b:** MnS (dark) and pearlite in low carbon steel viewed at high magnification as revealed by metallographic preparation, chemical etching, and optical microscopy (Sauveur, 1912).

mond and Le Chatelier in France, and others, revealed the microscopic structure of steel and other industrial alloys. These advances were enabled by the development of the optical microscope to very nearly its modern level of performance. Researchers pursuing the techniques that came to be known as "metallography" learned how to perform careful mechanical polishing of metallic alloys followed by selective chemical etching to produce differential relief on chemically distinct phases or at grain boundaries. With such specimens, reflection optical microscopy revealed structures with micrometer and even finer dimensions. Examples of the excellent quality of their images of metallographically-prepared iron-based and Cu-Ag alloys are shown in Figures 1 and 2. The microstructural world that was found proved to be highly complex, and most alloys were observed to be chemically differentiated into two or more distinct phases. In a short time, what has become the central paradigm of modern materials science was recognized, namely that the

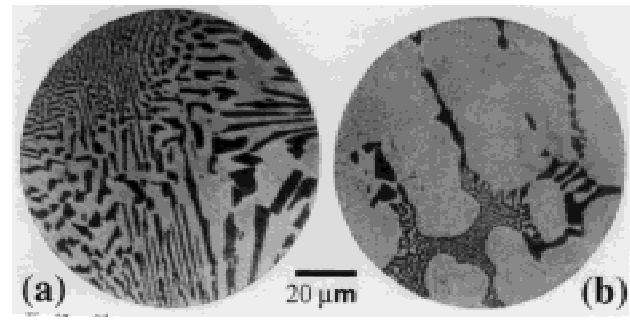

Figure 2. Ag-Cu alloys: (**a**) Ag-28 wt% Cu; (**b**) Ag-65 wt% Cu as revealed by metallographic preparation, chemical etching, and optical microscopy (Sauveur, 1912).

microstructure of a material had a profound, often controlling, impact upon macroscopic properties and behavior. Control of the microstructure meant control of critical properties such as strength, hardness, ductility, corrosion resistance, etc. In his introduction to his 1912 book, *Metallography of Iron and Steel,* Albert Sauveur, Professor of Metallurgy and Metallography at Harvard University, noted:

> To realize the practical importance of metallography, it should be borne in mind that the physical properties of metals and alloys—that is, those properties to which those substances owe their exceptional industrial importance—are much more closely related to their proximate than to their ultimate composition, and that microscopical examination reveals, in part at least, the proximate composition of metals and alloys, whereas chemical analysis seldom does more than reveal their ultimate composition. (Sauveur, 1912)

Here the "ultimate composition" is what we today would refer to as the bulk composition, while the "proximate composition" refers to the local microstructural composition. Sauveur continued in his enthusiastic and colorful prose:

> Unfortunately the chemist too often is able to give us positive information in regard to the proportion of the ultimate constituents only, his reference to proximate analysis being of the nature of speculation. Ultimate analysis has reached a high degree of perfection in regard to accuracy as well as to speed of methods and analytical chemists have built up a marvelous structure calling for the greatest admi-

> ration, their searching methods never failing to lay bare the ultimate composition of substances. **But how much darkness still surrounds the proximate composition of bodies and how great the reward awaiting the lifting of the veil!** [boldface added] (Sauveur, 1912)

This "lifting of the veil" would take 39 more years after Sauveur's impassioned plea for the arrival of Castaing's electron probe, fully described in his thesis to the University of Paris in 1951 (Castaing, 1951). This thesis, like Gaul itself, is divided into three parts. It is first an instrumentation thesis, in which he develops a working electron probe instrument that operates as an analytical tool with 1 μm spatial resolution. In the second part, Castaing describes the theoretical basis for quantitative electron microprobe analysis from X-ray intensity measurements. This carefully reasoned development of the theory of electron-excited X-ray production and propagation formed the foundation for all subsequent work in the field. Finally, the third part of the thesis demonstrates the practical nature of the electron probe through carefully chosen examples of problem solving taken from metallurgy. In this paper, Castaing's demonstrations of applications in materials science will be considered, and the subsequent path of the electron probe microanalyzer in the development of materials science will be considered. This review will necessarily be cursory. A review with proper detail would fill an entire volume, so great has been the impact of electron probe microanalysis in materials science, as even a casual examination of the proceedings of the annual Microscopy and Microanalysis conferences will attest (Microbeam Analysis Society and Microscopy Society of America).

Castaing's Thesis Applications in Materials Science

Basic Materials Science Information Infrastructure: Determining Equilibrium Phase Diagrams

The equilibrium phase diagram is a basic tool of materials science, relating composition, temperature, and phase for two or more elemental or compound constituents, an example of which for copper and zinc is shown in Figure 3. Determining a phase diagram involves careful studies of the composition-temperature space with a series of alloys that span the full range of composition. These samples are allowed to equilibrate at a particular temperature and are either studied at that temperature in an appropriate measuring apparatus (e.g., a high temperature X-ray diffractometer) or else are rapidly quenched to room temperature, hopefully retaining the high temperature structure (Hansen, 1938/1958). Traditionally, this important work was carried out with chemical analysis to measure the bulk composition and X-ray diffraction to identify the crystalline phases, including solid solutions and intermetallic compounds. To measure the composition of the individual phases, workers attempted to grow sufficiently large crystals for bulk analysis. Alternatively, while working under a microscope, they carefully removed small chips of each distinct phase to accumulate enough for bulk analysis. Additional measurements, including hardness, electrical resistivity, magnetic properties, etc., were used to identify phase changes associated with boundaries in the diagram.

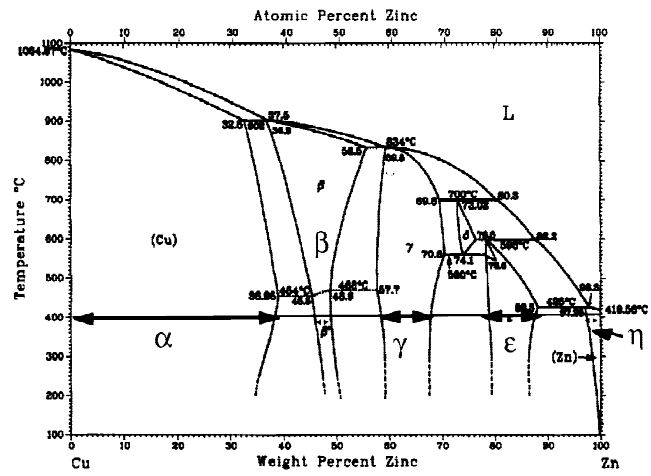

Figure 3. Equilibrium phase diagram for copper-zinc. The section through the phase diagram created by the Cu-Zn diffusion couple held at 400°C is shown (reprinted from Baker, 1992, with permission of ASM International). L, liquid.

The electron probe microanalyzer was clearly a tool that could revolutionize the determination of phase diagrams. Castaing devised a clever experiment to demonstrate the power of the electron microprobe for phase diagram work. He prepared a diffusion couple by creating an interface between two pure metals, copper and zinc, representing the end members in Figure 3. By holding this pure metal couple at a selected fixed temperature (400°C) for a fixed time (1 h) for diffusion to occur, reactions between Cu and Zn atoms produced the phases appropriate to that temperature horizon in the phase diagram. Thus, in a single specimen, a great deal of information about the phase diagram could potentially be measured if the measurement tech-

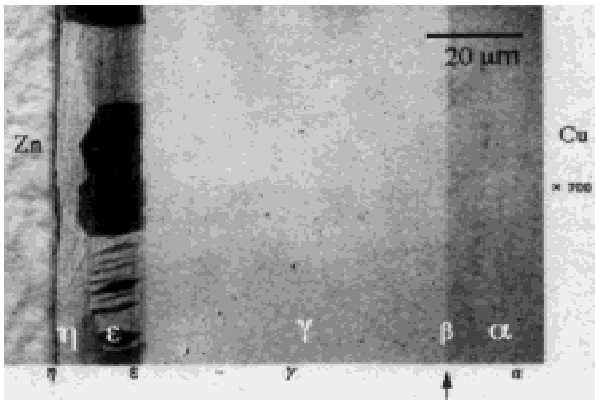

Figure 4. Polished section through Cu-Zn diffusion couple after 1 h at 400°C, as revealed by metallographic preparation and optical microscopy (reprinted with permission from Castaing, 1951).

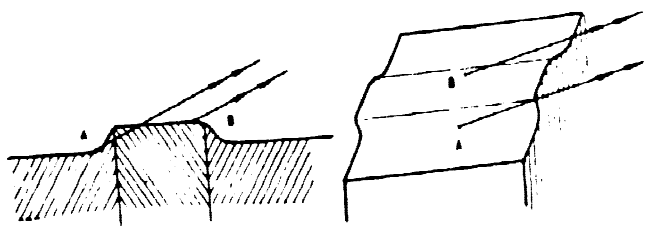

Figure 5. Proper orientation of diffusion couple to avoid anomalous absorption due to surface relief and to establish a consistent X-ray absorption path (reprinted with permission from Castaing, 1951).

nique had sufficient spatial resolution. The Gibbs phase rule dictates the form of the specimen that results from such an experiment. For an experiment in which pressure is a constant, the Gibbs phase rule becomes:

$$F = C - P + 1 \qquad (1)$$

where C is the number of components (C = 2 for the Cu-Zn binary), P is the number of phases present, and F is the number of degrees of freedom (or independent variables that can be varied without disturbing the system equilibrium). For two components and two phases, F = 1, and with position in the diffusion couple as a variable (varying perpendicular to the original interface), a two-phase region in the phase diagram is constrained as a planar interface between pure phase regions. For two components and one phase, F = 2, and again with position in the diffusion couple as a variable, a single phase region in the phase diagram is found to have a finite width parallel to the diffusion direction. This imposed condition explains the form of the diffusion sample cross section, shown in Figure 4, where each of the single phase regions noted in Figure 3 (except for the β phase) is found as one of the bands of varying width in the image.

The labeling of the phases in Figure 4 is based upon Castaing's quantitative electron probe analysis of the section. Before proceeding with this analysis, Castaing noted the importance of carefully selecting the orientation of the spectrometer relative to the specimen, emphasizing the need to measure X-rays along a line parallel to the original diffusion interface, as shown in Figure 5. This orientation eliminated possible anomalous X-ray absorption which could occur due to surface relief developed during polishing of phases with different hardnesses. Such an orientation also ensured that the X-rays passed through material of constant composition, thus that any compositionally based corrections, such as for absorption, would be consistent. Castaing's measurements are shown in Figure 6, where the measured *k*-values (relative to pure elements) are plotted as a function of position. For this particular case, Castaing noted the near absence of any matrix corrections because of the similar atomic numbers of copper and zinc, and the low values of the mass absorption coefficients for Cu*K*α and Zn*K*α. Thus, to a close approximation, the *k*-values are equivalent to concentrations. Examination of the concentration profiles reveals that the concentrations correspond well with the values taken from the published equilibrium phase diagram for the α, γ, ϵ and η phases, each of which shows a region of composition varying with position, which is consistent with the range of compositional stability previously found by the classical methods. The apparently missing β phase was in fact observed as a very narrow layer less than 1 μm thick, which was below the resolution of Castaing's first electron probe microanalyzer. This example demonstrated both the power of the electron probe to gather a great deal of data, characterizing an entire isotherm in a single experiment, and also the limitations imposed by the kinetics of phase formation, which along with the diffusion coefficient in each phase determined the thickness of each distinct phase zone. It clearly pointed out the need for even better spatial resolution than the micrometer level achieved with Castaing's thesis instrument, a theme that continues to this day.

The actual impact of Castaing's demonstration of the potential of the electron probe for phase diagram studies upon materials science took about 15 years, a time period during which the commercial electron microprobe instruments were acquired by various materials science laborato-

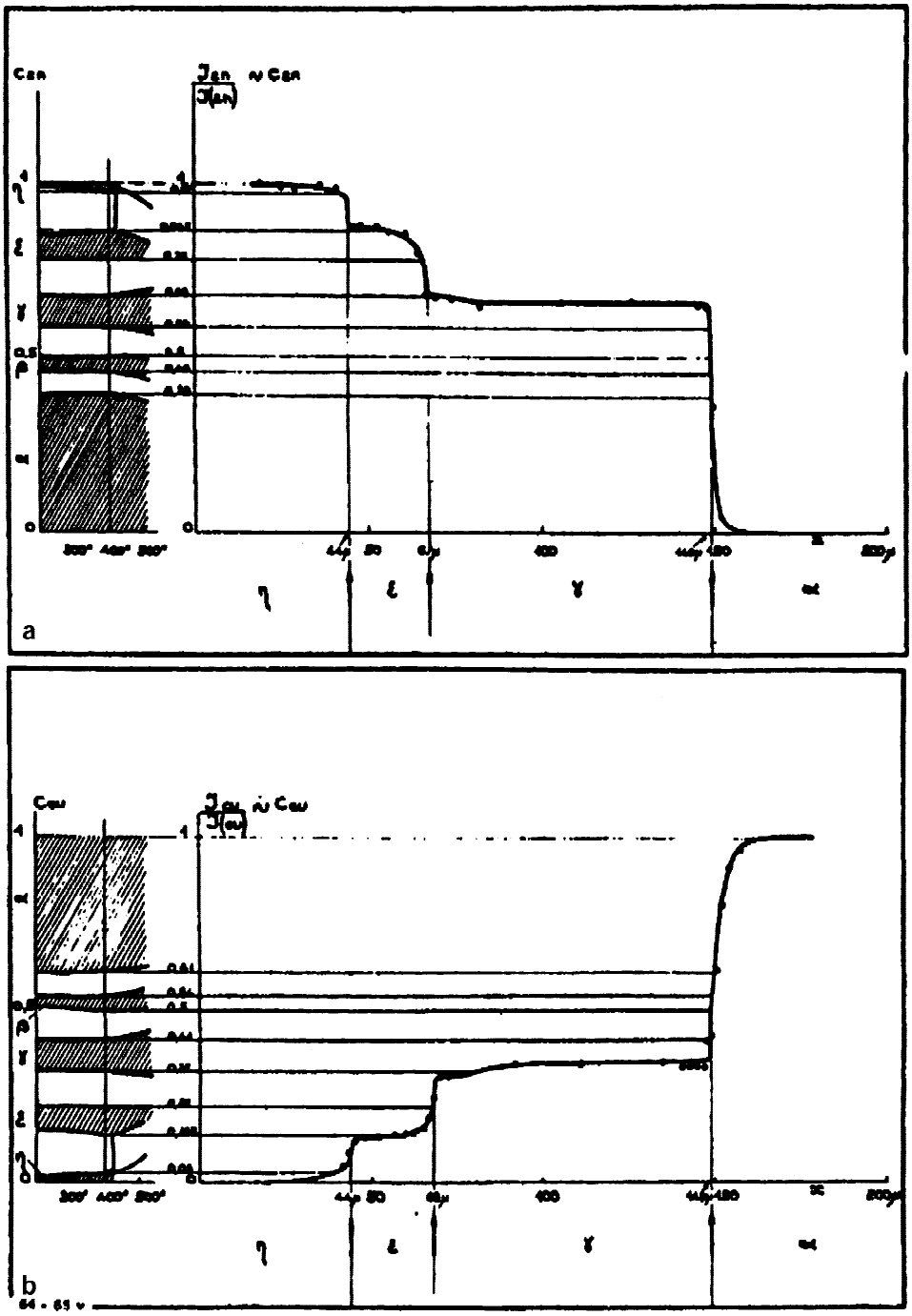

Figure 6. *k*-Values for Zn (**a**) and Cu (**b**) vs. position in the diffusion couple (reprinted with permission from Castaing, 1951).

ries and confidence in the analytical methods was developed. The great compendium of phases diagrams was that compiled by Max Hansen in 1936 and updated in 1958 (Hansen, 1936/1958). The 1958 volume includes references up to 1955, and the analytical techniques mentioned include X-ray diffraction, metallography, bulk chemical analysis, including analysis of shavings from pure phases, hardness, resistivity, magnetic properties, etc. The 1965 update by Elliott includes information derived from the same suite of characterization techniques (Elliot, 1965). By the time of the 1969 update by Shunk, which includes references as late as 1967, electron microprobe measurements are specifically identified in the new information contributing to the redrawing of a number of binary phase diagrams, including Ag-Be, Ir-Mo, Ni-Zr, Pu-Y, and Si-U (Shunk, 1969).

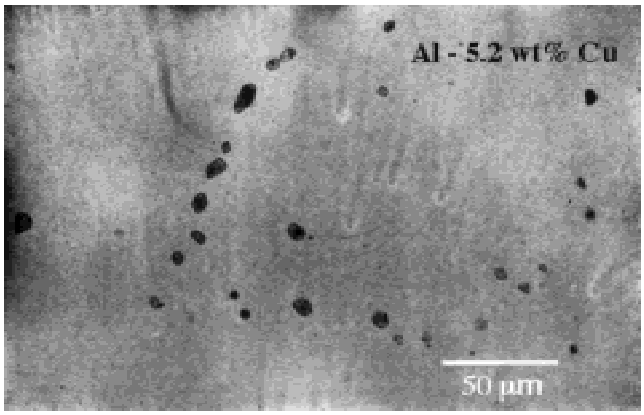

Figure 7. Precipitates grown in Al-5.2 wt% Cu alloy as revealed by metallographic preparation, chemical etching, and optical microscopy (reprinted with permission from Castaing, 1951).

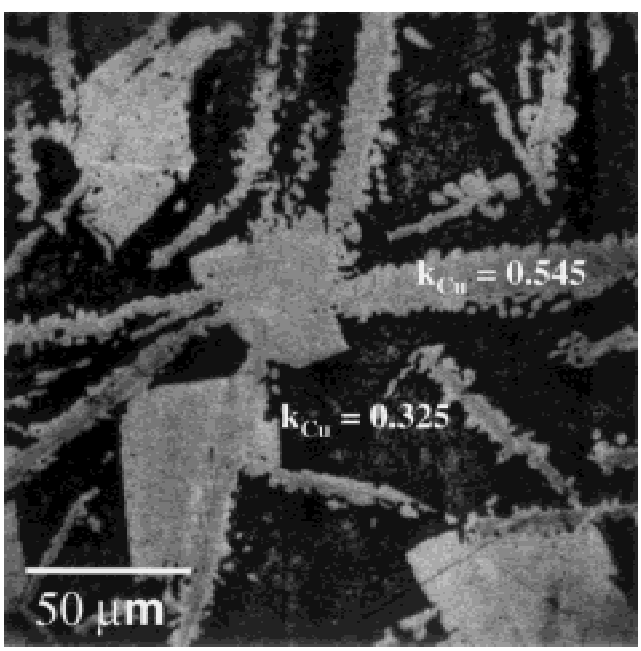

Figure 8. The microstructure of Cu-Sn-Sb alloy as revealed by metallographic preparation, chemical etching, and optical microscopy (reprinted with permission from Castaing, 1951).

Breaking New Ground: Analysis of Alloy Microstructures

The Cu-Zn diagram example was a powerful indication of the potential role for the electron probe microanalyzer for phase diagram determination and the measurement of diffusion coefficients. Castaing noted that, compared to traditional analytical methods for studying diffusion (e.g., chemical or electrochemical etching, microhardness, or radioactive tracers), the electron probe approach

> . . . becomes remarkably simple and rapid. . . . However in this field of application of electron probes, this new method only replaces, with advantage, the existing methods. Other fields of application in research, however, cannot be studied at all except by this new method. Let us mention, for example, the study of local variations of concentration inside an alloy and especially the analysis of segregations, precipitates, or inclusions of unknown or incompletely known nature. (Castaing, 1951)

With this introduction, Castaing proceeded to demonstrate the power of the electron probe microanalyzer for local analysis of discontinuous phases present in a matrix. He chose the alloy Al-5.2 wt% Cu, which after heat treatment revealed discontinuous precipitates with a range of sizes, as shown in Figure 7. The spectrometer used in his thesis research did not have the range to reach the long wavelength Al*K*α X-rays, so Castaing was forced to make inferences based solely on measurements of the Cu*K*α peak. He first observed that for a beam energy of 30 keV, a plot of k_{Cu} vs. precipitate size was constant down to a diameter of approximately 3 μm, below which size the beam penetration through the particle caused the *k*-value to decrease with further reductions in precipitate diameter. Thus, precipitates above this size could be analyzed quantitatively, and he found that the value of k_{Cu} was consistent with that measured from large crystals of Al_2Cu. He noted that qualitative analysis, that is, recognition of the constituents, was still possible with his electron probe microanalyzer for precipitates with diameters as small as 0.5 μm. Quantitative analysis of Cu in the Al-Cu system involved matrix corrections and was carried out based upon the α-factor method discussed by Castaing earlier in the thesis in his development of analytical methods. This procedure relied on developing the relation between C_i and k_i with alloys of known composition. For the Al_2Cu intermetallic, the correction C/k = 0.525/0.504 = 1.042.

Castaing then extended his study of precipitates to the Cu-Sn system, a metallographic specimen of which is shown in Figure 8, where he was again hampered by the limitations of his spectrometer. Sn*K*α and Sb*K*α were too short in wavelength, while Sn *L*α and Sb *L*α were too long for mea-

Table 1. Castaing's Analysis of Phases in Cu-Sb-Sn Alloys

Variable	k_{Cu}	C_{Cu}	Absorption correction	Phase	Cu_{phase}
Bright phase	0.545	0.618	1.13	Cu_3Sn	0.616
Dark phase	0.325	0.396	1.22	Cu_5Sn_4	0.401

surement, leaving only CuKα available. Again, careful inference as well as correlated measurements on synthetic crystals were necessary to achieve a meaningful quantitative analysis because of a large absorption correction. Based upon his careful theoretical development of the absorption correction, Castaing was able to accurately correct the measured *k*-values for the phases measured in Figure 8. The results are listed in Table 1, where the concentration values determined from corrections of the measured intensities correspond very well with stoichiometric intermetallic phases found in this system.

Further Developments

Following the presentation of his thesis, Castaing continued to work diligently with various colleagues and students to advance electron microprobe instrumentation, to improve the correction schemes for quantification, and to demonstrate applications of the electron microprobe to materials science. An expanding community of researchers in many countries contributed their efforts to advancing the field, aiding the broad acceptance of the electron microprobe in materials science. One of the most significant advances of the 1950s outside of Castaing's laboratory was the scanning electron microprobe of Cosslett and Duncumb (1956) and their demonstration of the technique of X-ray mapping. Most important to actual use was the development of practical commercial instruments by several manufacturers in Europe, the United States, and Japan, which brought the technique to the broader community of users. By the time the first National Conference on Electron Probe Microanalysis was held in the United States in 1966 at College Park, MD, the electron probe microanalyzer was becoming a critical tool for materials science. The proceedings of the this conference (Marton, 1966) includes numerous examples of advanced applications of the electron microprobe to materials science, including analysis of: (1) refractory metal coatings (P. Lublin and W. Sutkowski); (2) diffusion in the Ti-Nb system (D. Nagel and L. Birks); (3) Au-Al alloys (C. Nealey); (4) various steels (H. Nikkel); (5) Al-V-Mo-Ti alloys (R. Olsen); (6) corrosion of Ni-Co alloy (C. Spengler and R. Stickler); and (7) analysis of metal oxides and carbides (T. Ziebold).

Following 1966, four further developments in instrumentation had a profound effect on the impact of electron probe microanalysis, especially in materials science. (1) The development from 1948–1965 of the scanning electron microscope (SEM) as a practical instrument by Prof. Sir Charles Oatley and his many students provided high resolution imaging in an instrumentation platform that could also be equipped for electron beam microanalysis activities (Oatley, 1972, 1982). The late 1960s and early 1970s saw a tremendous growth in the number of laboratories equipped with SEMs. (2) This evolutionary trend was immeasurably stimulated by the development of the semiconductor energy dispersive X-ray spectrometer (EDS), which permitted the ready acquisition of X-ray spectra while permitting the full performance of SEM imaging (Fitzgerald et al., 1968). While extraordinarily well suited for rapid qualitative analysis, EDS was subject to numerous peak interferences and poor detectability because of its poor spectral resolution compared to wavelength dispersive spectrometry (WDS). The highly complementary nature of EDS and WDS logically lead to combined EDS/WDS on a high performance SEM platform augmented with optical microscopy (OM) for optimal operation of the WDS. SEM/OM/EDS/WDS thus led to a powerful combination instrument with high resolution imaging and virtually uncompromised X-ray spectrometry (Goldstein et al., 1992). (3) The third development was the frenetic revolution in computing power which led to computers dedicated to individual experimental devices. The electron probe X-ray microanalysis field, through individual researchers as well as commercial enterprises, was an eager and highly effective user of the new computing technology. As each wave of computer technology swept through with advancing computational power, speed, and mass storage, the electron probe microanalysis field quickly adopted every advance to implement true computer-assisted analysis and microscopy, thus enormously increasing the power and efficiency of the instrumentation. (4) The fourth development directly attacked the problem of the limitation on spatial resolution imposed by the scattering of the beam electrons in thick targets. Castaing and Henry (1962) and Castaing (1975) explored the application of electron energy loss spectrometry (EELS) with a magnetic prism in the transmission electron micro-

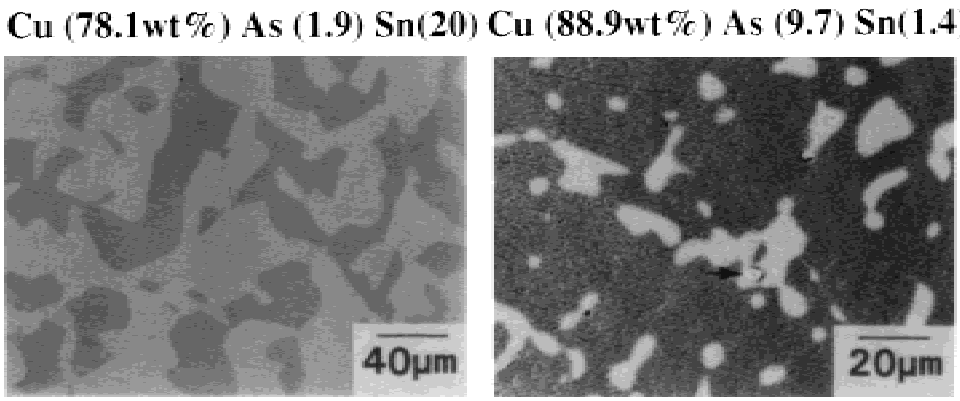

Figure 9. Backscattered electron (BSE) scanning electron microscopy (SEM) images of two Cu-Sn-As alloys showing phases present in alloys heat-treated at 570°C (Roeder and Notis, 1985).

Table 2. Phase Composition Determined by Quantitative Electron Probe Microanalysis[a]

Phase	Cu (mass fraction)	As (mass fraction)	Sn (mass fraction)
α (α + γ field)	0.853 ± 0.02	0.0240 ± 0.0054	0.123 ± 0.0093
γ (α + γ field)	0.737 ± 0.017	0.0154 ± 0.0054	0.247 ± 0.011
α (α + Cu_3As field)	0.912 ± 0.0025	0.072 ± 0.0065	0.0159 ± 0.0015
Cu_3As (α + Cu_3As)	0.719 ± 0.0022	0.279 ± 0.012	0.0014 ± 0.0024

[a]Mean value; the error represents two standard deviations for a set of 10 replicate measurements.

scope, a route to high spatial resolution analysis that would flower in the 1990s with the development of parallel EELS detection systems and high brightness field emission sources (Egerton, 1996). The X-ray spectrometry route to high spatial resolution was pioneered by Duncumb, who devised the electron microscope microanalyzer (EMMA), which has evolved into the commercial analytical electron microscope (AEM) (Duncumb, 1968; Williams and Carter, 1996). The AEM is based upon a high resolution transmission/scanning transmission electron microscope operating at high beam energies, 100 to 400 keV. With a thin foil specimen (<100 nm thick), the AEM provides an improvement in spatial resolution by a factor of 5 to 100 over the electron microprobe with a thick specimen of the same composition. Far advanced from the initial concept of a single-technique microanalysis instrument, the modern AEM incorporates, in addition to X-ray spectrometry, the EELS technique as well as a complete suite of diffraction methods. The result is a complete characterization tool that is capable of observing atomic scale morphology complemented by nanometer-scale compositional and crystal structure measurements. The modern SEM/electron probe microanalyzer (EPMA) and the AEM have thus achieved the status of critical tools in the arsenal of materials science characterization.

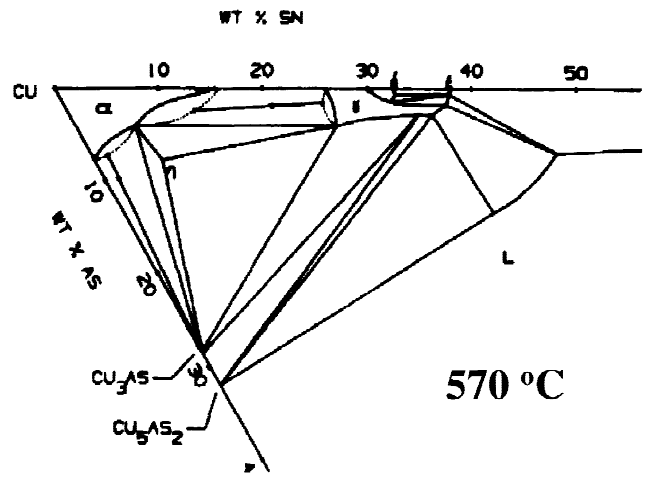

Figure 10. The redrawn Cu-Sn-As ternary phase diagram at 570°C based upon critical quantitative electron probe measurements (Roeder and Notis, 1985).

Examples of Electron Probe Microanalysis in Modern Materials Science

A few examples of recent applications of electron probe microanalysis in materials science will serve to illustrate the

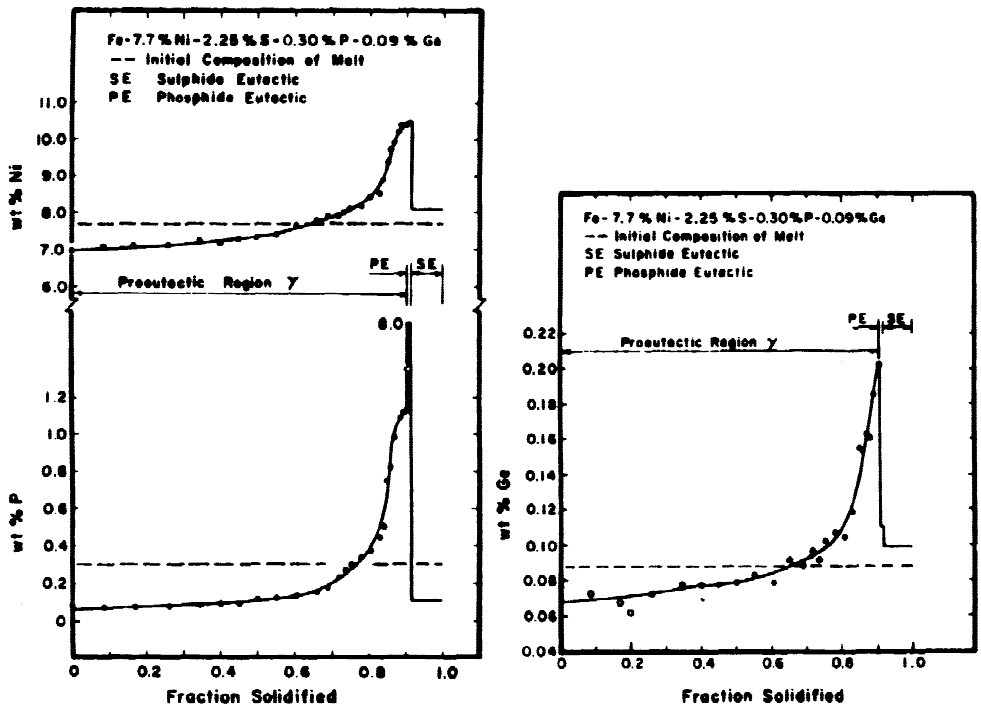

Figure 11. Plots of the concentrations of Ni, P, and Ge in directionally solidified melt-grown crystals of Fe-Ni alloys. Note the low concentration levels of P and especially Ge which are achieved with robust statistics (Sellamuthu and Goldstein, 1984).

power of the modern SEM/EPMA/AEM instruments. The article of Roeder and Notis (1985) serves as a modern example of the *routine* application of the electron probe to phase diagram determination. In this case, the authors needed to redetermine a portion of the ternary phase diagram for Cu-Sn-As in support of archeological studies, working in the copper-rich portion of the diagram. These authors prepared two different alloy compositions and heat treated them at 570°C for a sufficient time to approach equilibrium, at which point the specimens were quenched to room temperature to preserve the high temperature phase equilibria. Backscattered electron images in the modern scanning electron microscope/microprobe revealed the phases present, as shown in Figure 9. Quantitative electron probe microanalysis was employed to determine the phase composition, the results of which are given in Table 2. From these electron probe measurements and other data, the authors were able to redraw the Cu-Sn-As ternary phase diagram, as shown in Figure 10.

As an example of high sensitivity measurements, the article of Sellamuthu and Goldstein (1984) describes a study of the redistribution of various solutes in iron-nickel alloys during directional solidification to create melt grown crystals. Several of their results for Ni, P, and Ge are shown in Figure 11. The horizontal axis in each graph represents the fraction of the specimen that had solidified at a given point in the directional solidification process. The tendency of the solutes to be rejected from the solid into the liquid is clearly shown in these figures. Most impressive is the quality of the data obtained in this study. Note particularly the results for Ge, which ranges in concentration from 0.0007 to 0.0021 mass fraction, where sufficient X-ray counts above background were accumulated to reduce the statistical scatter to a negligible fraction compared to the actual modulation of the concentration due to the physical phenomenon.

An example of a particularly challenging measurement which is supported by independent chemical measurements is reported in the work of Galli and Gumz (1991). Carbon is a difficult element to measure, especially at trace levels. The measurement of carbon is particularly complicated because of its ubiquitous nature in sample preparation materials, and because of the tendency for carbon to deposit at the specimen surface in the beam impact area, due to electron beam-induced cracking of hydrocarbons present as contamination preexisting on the specimen surface or as a residual gas in the vacuum system. In the results shown in Figure 12, carbon contamination was suppressed by the use of a liquid nitrogen cooled cold finger and a defocused (30 μm) beam to reduce the current density. Figure 12a shows a linear "working curve" of the net carbon intensity above background, measured as a function of composition for iron and two iron-nickel alloys. Using the working curve,

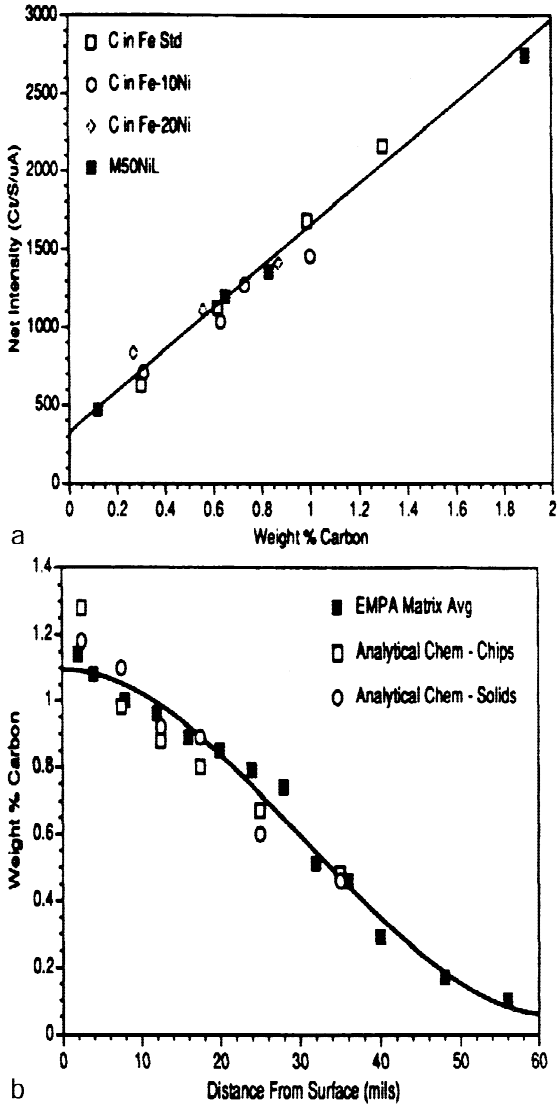

Figure 12. **a:** Plot of the "working curve" of the measured carbon intensity above background as a function of concentration in iron and two iron-nickel alloys. **b:** Comparison of carbon analyses by electron microprobe and wet chemical analysis of chips ground from the surface as a function of depth (in mils = 25.4 μm) in a carburized Fe-4Cr-4Mo-1V-3.5Ni (Galli and Gumz, 1991). EMPA, electron microprobe analyzer.

Figure 12b shows the carbon profile in a cross section taken perpendicular to carburization surface. Most importantly, Figure 12b also shows the results of independent wet chemical analyses performed on chips taken by grinding parallel to this surface. The correspondence between electron microprobe analysis and wet chemical measurements is very close. Such testing of electron probe microanalysis whenever possible with other techniques was much more common in the early history of the field, and although such independent studies are often difficult, it is important to continue such testing today to ensure the rigor of our analyses.

The improvement in analytical spatial resolution obtained with the AEM on a thin specimen compared to the SEM/EPMA with a thick specimen is well illustrated in Figure 13 by the work of Miyake and Goldstein (1974) and Romig and Goldstein (1979). This is some of the earliest quantitative profiling work reported with a "modern" AEM. The improvement in analytical spatial resolution of measurements across α–γ interfaces by AEM compared to that achieved with the EPMA is at least a factor of 5 (step size 50 nm in AEM vs. 250 nm with EPMA), but the abruptness of the interface in the AEM profile suggests that the true spatial resolution is improved by at least a factor of 20. With the improved resolution in the AEM, an actual gradient in the nickel concentration at the α–γ interface can be observed.

Failure analysis is one of the most important areas of application of the electron probe microanalyzer, requiring the analyst to take on the role of a sleuth to solve problems. The impact of failure analysis applications ranges across the entire field of materials science, into the processes by which products are produced, and into the failures of those products. In parallel with the central paradigm of materials science, we often observe that a macroscopic system such as a complex multifunction device can undergo an unexpected failure due to a microstructural fault, introduced either from the basic starting material, during the manufacturing process, or as a result of the interaction of the product with its operating environment. This is especially true for the complex electronic devices, which may involve hundreds to thousands of manufacturing steps. As an example of a common macroscopic system failure mediated by microscopic events, consider the service failure of aluminum wiring in ordinary household electrical outlets (Newbury, 1982). Figure 14 shows a test structure in which the connection of an aluminum wire to a steel screw is glowing red hot while passing a rated current of 15 A. Figure 15 shows cross sections at the Al-steel and Al-brass interfaces, along with analyses, while Figure 16 shows X-ray compositional maps of these regions. The analysis reveals the reaction of the Al and Fe, and the Al and brass (Cu, Zn), to form intermetallic compounds. Such compounds are found to have much higher resistivity than the component Al wire and the steel and brass alloys that make up the connection. The higher

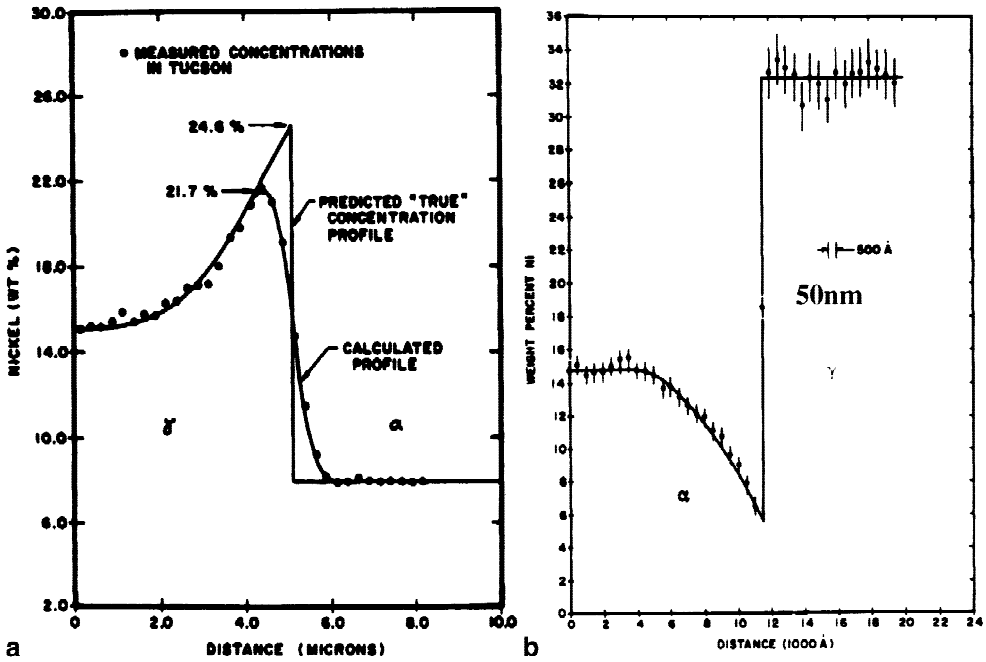

Figure 13. Measurements of the concentration of nickel across the α–γ interface in meteorites: **(a)** electron probe microanalyzer by Miyake and Goldstein, 1974 (note the deviation of the measured curve from the predicted "true" concentration profile from diffusion modeling); **(b)** analytical electron microscopy by Romig and Goldstein, 1979 (note much improved spatial resolution by at least a factor of 20, and detection of a true concentration profile near the α–γ interface).

resistivity leads to increased heat generation at the junction, raising the temperature and driving the intermetallic reactions forward in a case of positive feedback, leading to ultimate service failure. Thus, a microscopic fault progressively led to a macroscopic failure. The contribution of electron probe microanalysis to elucidating this microstructural mechanism was critical.

Future of the Electron Probe Microanalyzer in Materials Science

The future of electron probe microanalysis and analytical electron microscopy in materials science seems limitless. Even at the level of performance of our current instrumentation derived from Castaing's original electron probe, there seems to be no end to materials characterization problems as well as failure analyses that will continue to challenge our capabilities. Quite unexpectedly, however, there now appears to be the possibility of remarkable advances in instrument performance in the near future. While the instrumentation development seemed to be quite mature just a few years ago, research is pointing toward marvelous new capabilities.

In the area of the electron beam columns, the rapid advance of high performance field emission gun scanning electron microscopes (FEG-SEMs) makes possible the routine use of low beam energy (arbitrarily, <5 keV) microscopy and microanalysis, where analytical resolution of 30 to 100 nm can be achieved in bulk specimens. Commercial FEG-SEM instruments are already well established in the materials science field.

In the area of X-ray spectrometry, two exciting advances are developing in parallel. (1) The classic semiconductor EDS with a monolithic single crystal detector, which may have a volume as large as 180 mm^3, requires liquid nitrogen cooling for optimal resolution, and this resolution can only be achieved at modest count rates of 10 kHz or less. High count rate performance is usually limited to 25 kHz with deteriorated resolution. This performance may be greatly exceeded with the recently developed "silicon drift detector (SDD)" EDS, which utilizes a much different imposed electrical field configuration. The SDD EDS operates at much higher temperatures, approximately −20°C, which can be easily reached by thermoelectric cooling (Struder et al., 1999). The higher operating temperature and smaller anode of the silicon drift chamber design enable much shorter time constants (hundreds of nanoseconds rather than tens of microseconds). Consequently, count rates as high as 1 MHz have been achieved. Since these planar detectors can also be made large in area (several square centimeters), the large solid angle and high count rate capability should enable X-ray mapping in an energy dispersive mode to be performed at speeds never before possible, or alternatively, maps can be produced with much more rigorous counting statistics in the time now spent. (2) The

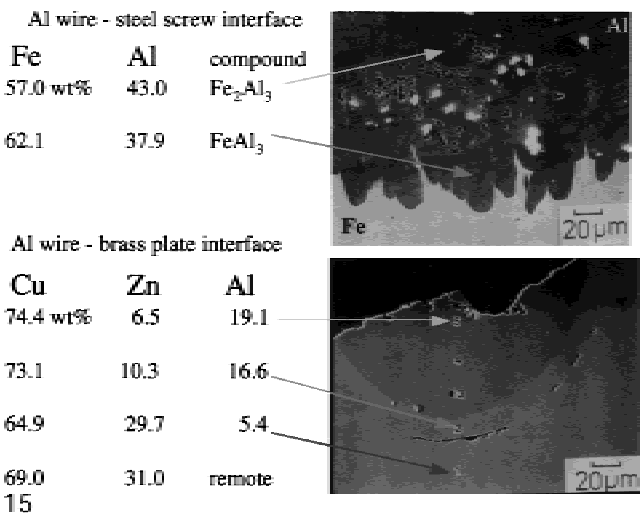

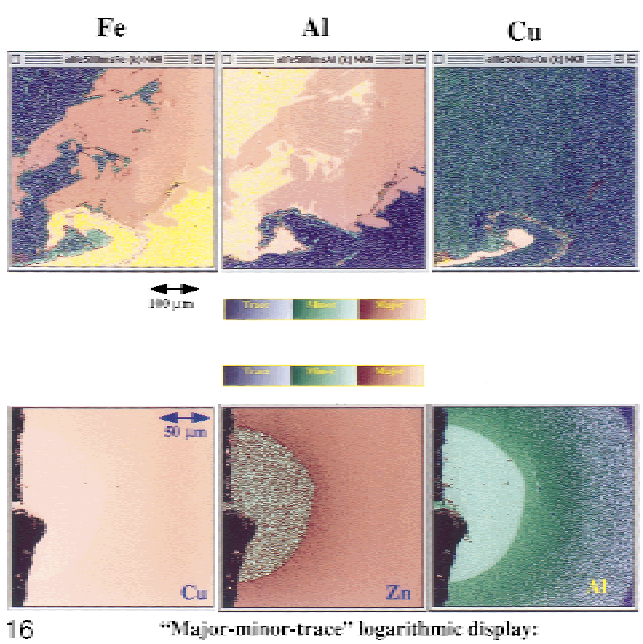

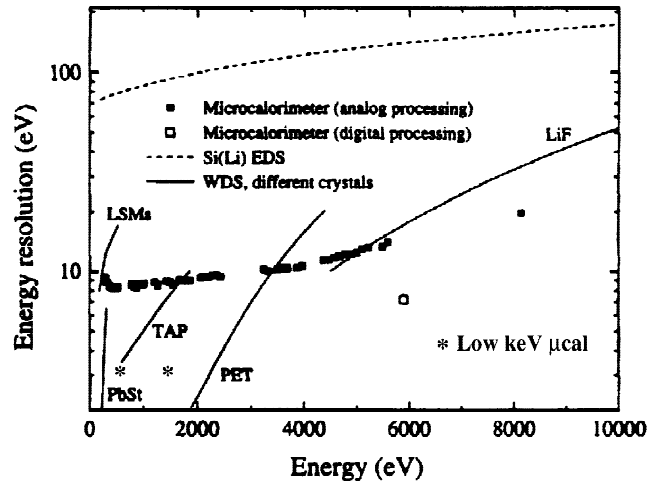

Figure 17. Resolution vs. photon energy for Si EDS (optimum resolution), WDS with various diffractors, and the NIST microcalorimeter EDS in its initial configuration (Wollman et al., 1997) and in a recent low photon energy version. EDS, energy dispersive spectrometry; NIST, National Institute of Standards and Technology; WDS, wavelength dispersive spectrometry; LSM, layered synthetic material; PbSt, lead stearate; PET, pentaerythritol; TAP, thallium acid phthalate.

second advance involves the development of microcalorimetry EDS, in which the physics of detection involves measuring the temperature rise generated by the absorption of an individual X-ray photon in a metal target (Wollman et al., 1997). As shown in Figure 17, the microcalorimeter can operate in an energy dispersive mode while achieving resolutions below 5 eV, with 2 eV possible for low energy photons below 2 keV in energy. The microcalorimeter EDS is already competitive with WDS over most of the photon energy range, and for low energy photons, it is much superior compared to the resolution of synthetic multilayer diffractors. Such high resolution combined with energy dispersive operation is critical for low beam energy microanalysis, where the low level of X-ray excitation and the limited access to atomic shells places severe demands on the per-

Figure 14. Aluminum wire connected to a steel screw and a brass pressure plate. The system is glowing red hot while passing a rated service load of 15 A.

Figure 15. Metallographic cross sections (SEM BSE images) of the reaction zones at the aluminum wire–steel screw interface and the aluminum wire–brass plate interface, with selected point analyses.

Figure 16. Compositional maps (*k*-values, not matrix corrected) of the reaction zones in the aluminum wire–steel screw–brass plate assembly from a household outlet assembly.

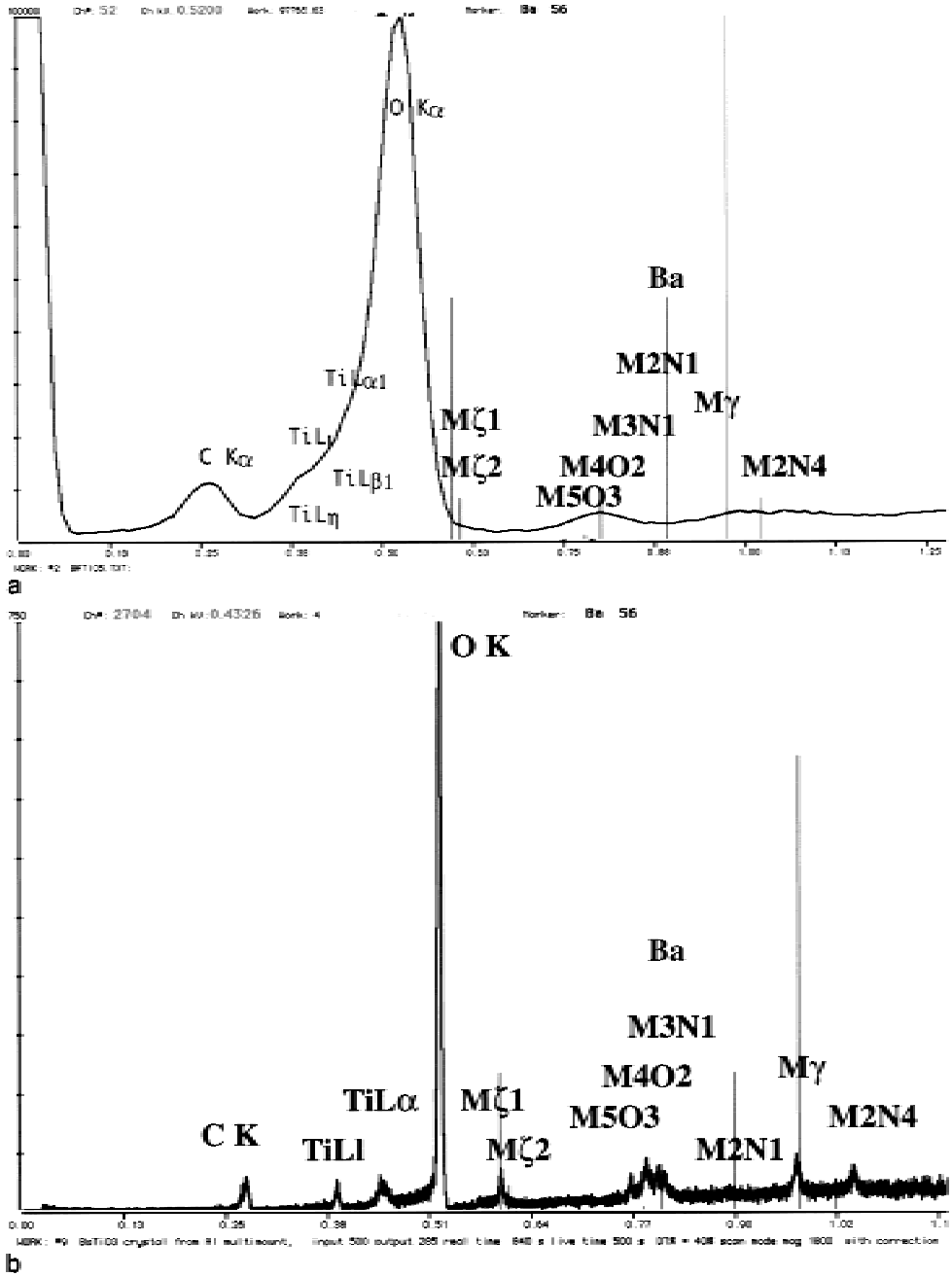

Figure 18. BaTiO3 with an incident beam energy of 3 keV: **(a)** conventional semiconductor (Si) EDS with 129 eV resolution (MnKα); **(b)** NIST microcalorimeter EDS.

formance of the spectrometer. For example, Figure 18 shows a comparison of barium titanate as measured with a conventional monolithic Si EDS (129 eV at MnKα) and with a microcalorimeter EDS. The microcalorimeter EDS can easily detect the Ti *L* and Ba *M* families.

The final area of development is that of crystallographic determination in the SEM/EPMA. Castaing made a considerable effort in his thesis to use Kossel patterns (diffracted characteristic X-rays generated in the specimen) for crystallographic studies. Although powerful, the Kossel technique never gained widespread popularity because of physical limitations and the procedural difficulty of using film in the chamber. Electron channeling patterns gave a much more rapid response, but the limited solid angle of the pattern, imposed by lens defects, limited the utility of this method (Joy et al., 1982). The problem of measuring crystal parameters from a broad range of practical sample types (e.g., flat surfaces, fracture surfaces, particles) has been solved by the technique of electron backscatter Kikuchi patterns (EBKP). EBKPs are created through diffraction

of elastically scattered, low energy loss electrons. The practical implementation of the EBKP technique has been greatly aided by the development of a high gain, large-solid angle camera and of automated processing with real-time computer-based methods. EBKPs have finally provided a robust crystallographic tool that is compatible with the imaging and spectrometry aspects of SEM/EPMA to yield a comprehensive characterization instrument for morphology, composition, and crystallographic phase information similar to the AEM (Michael, 1997).

Conclusions

Professor Raymond Castaing provided a great impetus to modern materials science with his development of the electron probe microanalyzer. When we realize that materials science is just one of many fields, including geology, biology, environmental science, forensic science, etc., where the microstructural characterization provided by electron probe microanalysis is critical to advancing basic scientific understanding, the extraordinary value of Professor Castaing's work can be appreciated.

References

Baker H (ed) (1992) Alloy phase diagrams. In: ASM Handbook, vol. 3. Materials Park, OH: ASM International, p 182

Castaing R (1951) Application of electron probes to local chemical and crystallographic analysis. PhD Thesis, University of Paris [English translation by P Duwez and DB Wittry, California Institute of Technology, 1955].

Castaing R (1975) Energy filtering in electron microscopy and electron diffraction. In: *Physical Aspects of Electron Microscopy and Microbeam Analysis,* Siegel B (ed). New York: Wiley, pp 287–301

Castaing R, Guinier A (1949) Application of electron probes to metallographic analysis. In: *Proceedings of the 1st International Congress on Electron Microscopy,* Delft, pp 60–63

Castaing R, Henry L (1962) Filtrage magnetique des vitesses en microscopie electronique. *C R Acad Sci* B225:76–78

Cosslett VE, Duncumb P (1956) Micro-analysis by a flying spot x-ray method. *Nature* 177:1172–1173

Duncumb P (1968) EMMA, combinaison d'un microscope electronique et d'une microsonde electronique. *J Microsc* 7:581

Egerton RF (1996) *Electron Energy-loss Spectroscopy in the Electron Microscope.* New York: Plenum Press

Elliott RP (1965) *Constitution of Binary Alloys, First Supplement.* New York: McGraw-Hill

Fitzgerald R, Keil K, Heinrich K (1968) Solid-state energy-dispersive x-ray spectrometer for electron probe x-ray analysis. *Science* 159:528–529

Galli F, Gumz K (1991) Electron microprobe analysis of carbon in carburized M5OniL. In: *Microbeam Analysis—1991,* Howitt DG (ed). San Francisco: San Francisco Press, pp 72–75

Goldstein JI, Newbury DE, Echlin P, Joy DC, Romig AD Jr, Lyman CE, Fiori C, Lifshin E (1992) *Scanning Electron Microscopy and X-ray Microanalysis.* New York: Plenum Press

Hansen M (1936/1958) *Constitution of Binary Alloys.* New York: McGraw-Hill

Joy DC, Newbury DE, Davidson DL (1982) Electron channeling patterns in the scanning electron microscope. *J Appl Phys* 53:R81–R122

Marton L (ed) (1966) *First National Conference on Electron Probe Microanalysis.* College Park, MD: Center of Adult Education, University of Maryland.

Michael JR (1997) All you need to know about electron backscatter diffraction: orientation is only the tip of the iceberg. In: *Microscopy and Microanalysis, Volume 3, Suppl. 2: Proceedings: Microscopy & Microanalysis '97, Cleveland, Ohio, August 10–14, 1997,* New York: Springer-Verlag, pp. 387–388

Miyake K, Goldstein JI (1974) The Tucson meteorite. *Geochim Cosmochim Acta* 38:1201

Newbury DE (1982) What is causing failures of aluminum wire connections in residential circuits? *Anal Chem* 54:1059A–1064A

Oatley CW (1972) *The scanning electron microscope: Part 1. The instrument.* Cambridge, UK: University Press

Oatley CW (1982) The early history of the scanning electron microscope. *J Appl Phys* R1–R13.

Roeder JF, Notis MR (1985) Electron microprobe determination of phase equilibria in the Cu-As-Sn system. In: *Microbeam Analysis—1985,* Armstrong JT (ed). San Francisco: San Francisco Press, pp 170–173

Romig A Jr, Goldstein JI (1979) Detectability limit and spatial resolution in STEM x-ray analysis: application to Fe-Ni alloys. In: *Microbeam Analysis—1979,* Armstrong JT (ed). San Francisco: San Francisco Press, pp 124–128

Sauveur A (1912) *The Metallography of Iron and Steel.* Boston: Sauveur and Boylston

Sellamuthu R, Goldstein J (1984) Segregation analysis of melt-grown crystals of Fe-Ni alloys with the use of the electron microprobe. In: *Microbeam Analysis—1984,* Romig AD Jr, Goldstein JI (eds). San Francisco: San Francisco Press, pp 303–306

Shunk FA (1969) *Constitution of Binary Alloys, Second Supplement.* New York: McGraw-Hill

Strüder L, Meidinger N, Stotter D, Kemmer J, Lechner P, Leutenegger P, Soltau H, Eggert F, Rohde M, Schulein T (1999) High-resolution X-ray spectroscopy close to room temperature. *Microsc Microanal* 4:622–631

Williams DB, Carter CB (1996) *Transmission Electron Microscopy: A Textbook for Materials Science.* New York: Plenum Press

Wollman DA, Irwin KD, Hilton GC, Dulcie LL, Newbury DE, Martinis JM (1997) High-resolution, energy-dispersive microcalorimeter spectrometer for x-ray microanalysis. *J Microsc* 188:196–223